Supporting Information

Pulse-Electrodeposited Ni-Fe (Oxy)hydroxide Oxygen Evolution Electrocatalysts With High Geometric And Intrinsic Activities At Large Mass Loadings

Adam S. Batchellor and Shannon W. Boettcher

Correspondence should be addressed to S.W.B.

swb@uoregon.edu

Table S1. Comparison of the geometric and intrinsic activities of Ni(Fe)OOH pulse deposited films to Ni(Fe)OOH films deposited onto more complicated supports.[1–4] Approximate values were either calculated via Tafel slope interpolation or read directly from Tafel data. We also note that these comparisons should be made with caution – differences in how iR correction is measured and applied, the reference electrode calibration, and the cell geometry, can easily change reported currents by a factor of 2 or 3.

Material: Ni(Fe)OOH	Pulse deposited on planar Au (this work)	Pulsed laser ablation onto pyrolytic graphite[1]	On reduced graphene oxide[2]	On Ni foam[3]	On carbon nanotubes[4]
J at η = 250 mV (mA cm^{-2})	8	~6	~42	~40	~ 40
J at η = 300 mV (mA cm^{-2})	120	~78	~75	300	~580
TOF at η = 300 mV (s^{-1})	0.42	~0.47	0.1	N/A	0.56
Loading (mg cm^{-2})	0.073	0.04	0.25	N/A	0.25

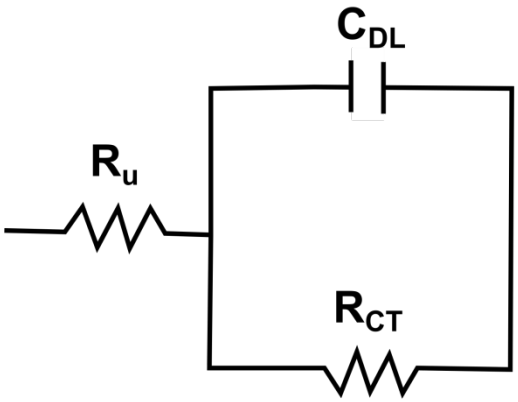

Figure S1. Equivalent circuit used to model the AC impedance of the electrochemical cell, with parameters including the uncompensated series resistance R_S, the charge transfer resistance R_{CT} and the double layer capacitance C_{DL}.

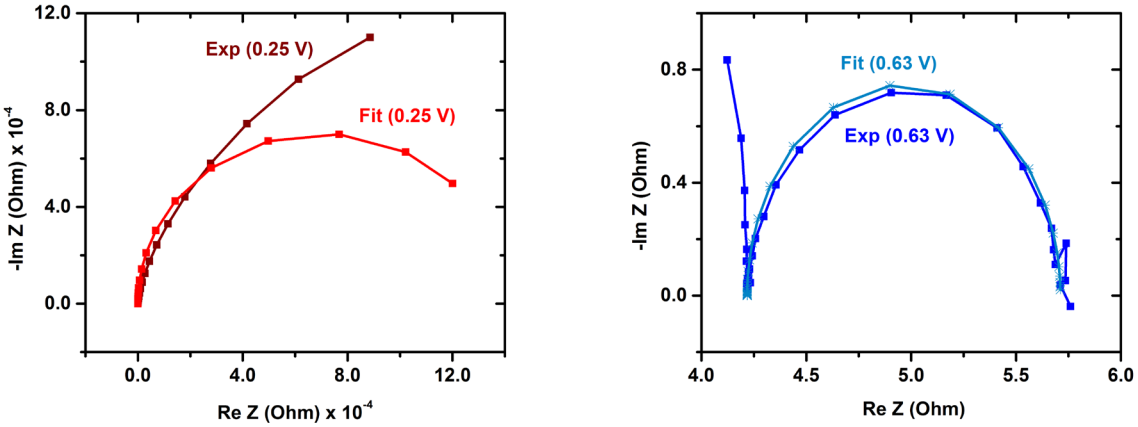

Figure S2. Impedance data showing the correlation of values obtained experimentally and through fitting at potentials corresponding to uncharged (0.25 V) and charged films (0.63 V). Least-squares data fitting was accomplished using software (EC Lab, Biologic). We note that the fits to the uncharged films are poor, suggesting a more-complicated circuit model is needed to fully capture the impedance response of the bare Au electrodes. This is in part due to the low capacitance of the bare electrodes. However, the conductive oxidized films are well fit by the simple circuit and it is these data – with several orders of magnitude higher capacitance – that are used to discuss catalyst loading.

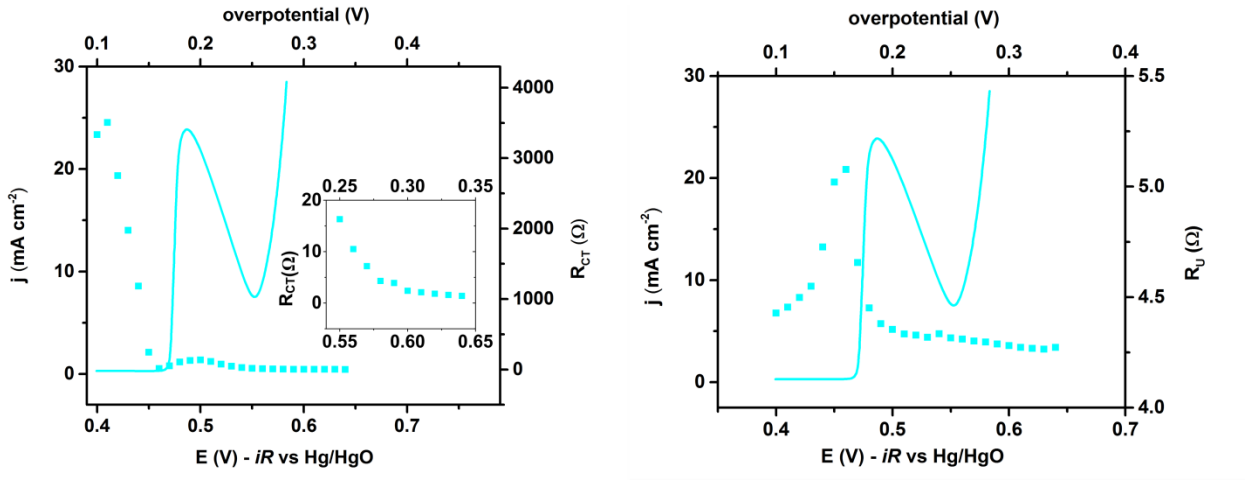

Figure S3. Voltammetry and the corresponding apparent charge transfer R_{CT} and uncompensated series R_U resistance values determined via AC impedance as a function of potential for the highest loading film on Au shown in Figure 2c. The data are representative of all film loadings examined. The small peak in R_U observed at potentials where the catalyst switches from an electrically insulating hydroxide to electrically conducting oxyhydroxide phase is likely an artifact of the simple equivalent circuit used that does not adequately model the system in this potential range where both capacitive charge of the underlying Au electrode, and faradaic charging of the $Ni(Fe)(OH)_2$/Ni(Fe)OOH film contributes substantially to the impedance response.

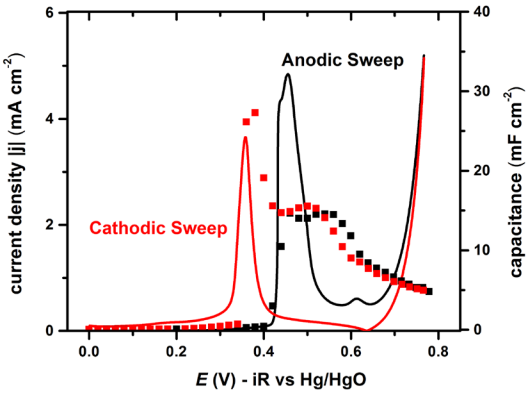

Figure S4. Impedance and voltammetry data from a NiOOH film (Fe free) showing correlation of capacitance and voltammetry data beyond the $Ni^{2+/3+}$ oxidation peak region highlighting the "turn on" and "turn off" of the film capacitance correlated with the change in Ni oxidation state.

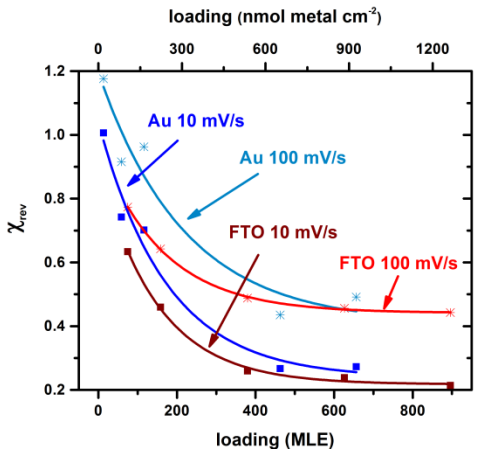

Figure S5. Reversibility values for continuously deposited films comparing the integrated areas of the anodic peak during the first cycle with the cathodic peak of the first cycle ($\chi_{rev} \equiv C_1/A_1$) for Au (blue) and FTO (red) electrodes at 10 (square) and 100 (star) mV/s. Notice that at 100 mV/s the reversibility is overestimated because the fast scan rate is too fast to measure all the charges in the first cathodic sweep.

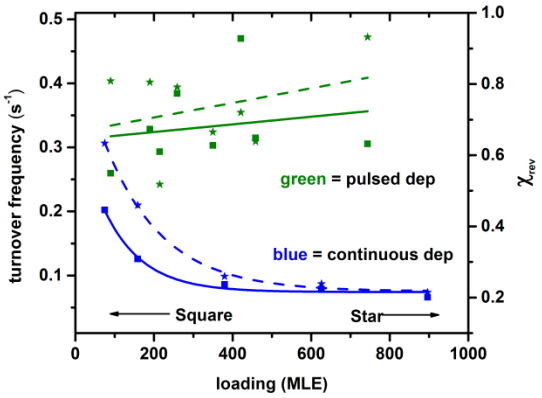

Figure S6. Loading-dependent behavior of catalyst films deposited on FTO substrates. Reversibility data (stars, dashed) and TOF data (squares, solid) are shown along with fit lines for continuously deposited films (blue) and pulse-deposited films (green). TOF data was obtained from chronoamperometry (iR_u corrected) and normalized with loadings determined using integration of the anodic peak on the first sweep for a fully reduced film.

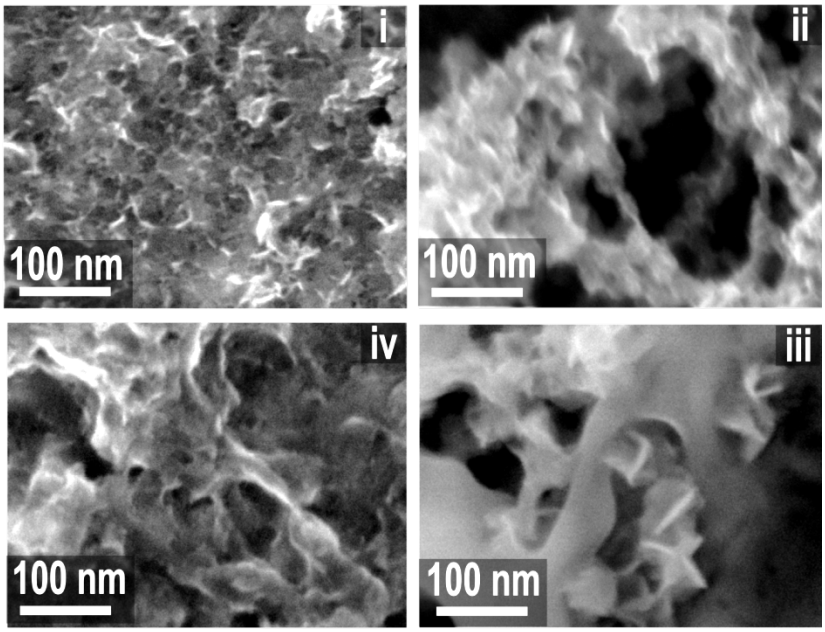

Figure S7. SEM images (top down) of thin (i,iv) and medium (ii,iii) loading films using continuous (i,ii) and pulsed (iii,iv) deposition. In 7i and 7ii, the development of the low packing density characteristic of high loading films becomes evident even by medium loading. In 7iii and 7iv, the extended sheets characteristic of pulse deposited films develop on the medium loading film.

Film Density Estimations:

Since electrochemical analysis was not performed on the films portrayed in the SEM images in this manuscript, density calculations are approximate. The loadings were taken from films deposited under similar conditions that underwent electrochemical analysis during which accurate loadings were determined. Films thicknesses were approximated from Figure 7.

Pulse Deposited: ~520 MLE / 300 nm = 1.7 MLE / nm

Continuously Deposited: ~660 MLE / 500 nm = 1.3 MLE / nm

Voltage Drop Calculations:

In order to estimate the voltage drop due to electrical resistivity of the film to expect for our thickest films, and thus the corresponding expected decrease in TOF, we used conductivity data collected previously.[5]

Using: (1) a conductivity value of 6 mS cm^{-1} for an approximately 15% Fe in Ni film, (2) a change in film thickness from the lowest to highest loading continuously deposited film of ~644 MLE (Figure 6), (3) a film density of 1.3 MLE/nm (from the above density calculation), and (4) a current density maximum of 50 mA cm^{-2}, the maximum electrical voltage drop can be estimated as shown below.

Maximum electrical voltage drop: $1/(6\ \text{mS cm}^{-1}) * 50\ \text{mA cm}^{-2} * 495 \times 10^{-7}\ \text{cm} = 0.4\ \text{mV}$

The expected change in TOF from Table S2 is then a factor of 1.03; negligibly small to measure experimentally.

To achieve the nearly 5 fold decrease in performance as shown in Figure 6, the average resistivity of the high loading films would need to be ~25 times greater than what was previously measured.

Table S2. Calculations showing expected decrease in current for various voltage drops based on film conductivity data previously reported assuming a Tafel slope of 35 mV/dec.[5]

Δ E (mV)	0	0.15	0.3	0.45	0.6	0.74	1.4	2.8	4	5.1	6.2	10.5	16.7	21.1	24.5	35
Δ TOF	1	1.01	1.02	1.03	1.04	1.05	1.1	1.2	1.3	1.4	1.5	2	3	4	5	10

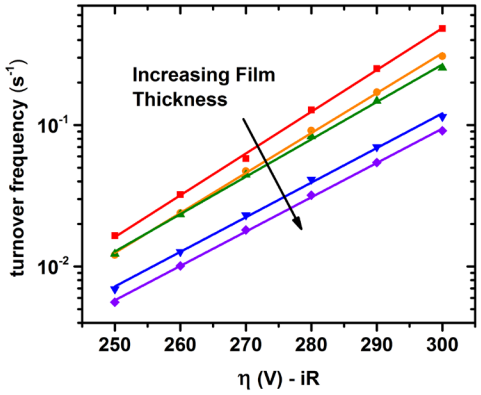

Figure S8. Tafel data for continuously deposited films on Au electrodes. Film thicknesses shown correspond to 13, 59, 116, 463 and 657 MLE. Current values were obtained from chronoamperometry (iR corrected).

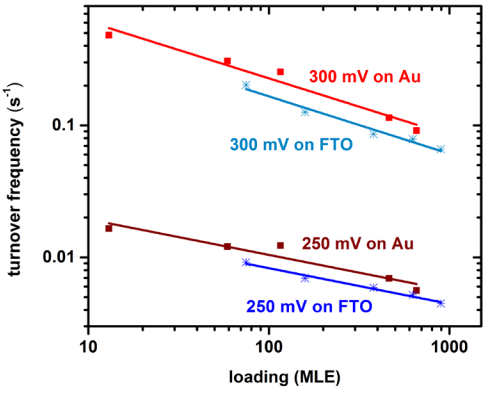

Figure S9. Activity of continuously deposited films showing the entire range of loadings for both substrates. Current values were obtained from chronoamperometry (iR corrected).

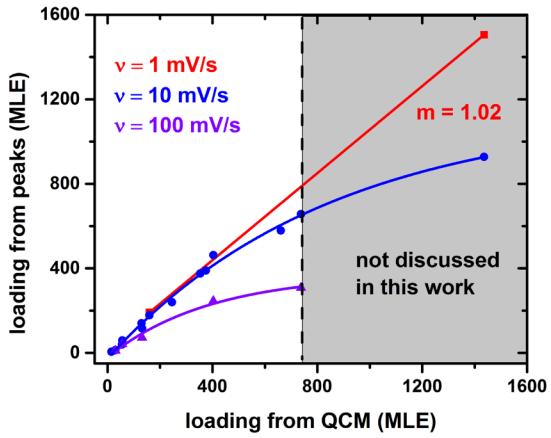

Figure S10. Comparison of loadings as determined by QCM and voltammetry at 1 mV/s (red squares), 10 mV/s (blue circles) and 100 mV/s (purple triangle). Peak integration of the $Ni^{2+/3+}$ redox features was completed on the first anodic wave recorded after fully reducing the film. The black dotted line at ~740 MLE (QCM) shows the highest loading film for which data was presented in the manuscript. At this loading, peak integration values calculated from voltammetry differ from those calculated via QCM by 11% and 59% for scan rates of 10 and 100 mV/s, respectively. It is therefore reasonable to use 10 mV/s over the loading range examined in this work. For even higher loadings, (e.g. ~1500 MLE), 1 mV/s scan rates are needed in order to measure all of the Ni's in the film.

Supplementary References

(1) Hunter, B. M.; Blakemore, J. D.; Deimund, M.; Gray, H. B.; Winkler, J. R.; Müller, A. M. *J. Am. Chem. Soc.* **2014**, *136*, 13118–13121.

(2) Ma, W.; Ma, R.; Wang, C.; Liang, J.; Liu, X.; Zhou, K.; Sasaki, T. *ACS Nano* **2015**, *9*, 1977–1984.

(3) Lu, X.; Zhao, C. *Nat. Commun.* **2015**, *6*, 1–7.

(4) Gong, M.; Li, Y.; Wang, H.; Liang, Y.; Wu, J. Z.; Zhou, J.; Wang, J.; Regier, T.; Wei, F.; Dai, H. *J. Am. Chem. Soc.* **2013**, *135*, 8452–8455.

(5) Trotochaud, L.; Young, S. L.; Ranney, J. K.; Boettcher, S. W. *J. Am. Chem. Soc.* **2014**, *136*, 6744–6753.